Accepted Manuscript

The nitro aromatic compounds detection by triazole carboxylic acid and its complex with the fluorescent property

Jie Yan, Jue Chen Ni, Jin Xin Zhao, Li Xian Sun, Feng Ying Bai, Zhan Shi, Yong Heng Xing

PII: S0040-4020(17)30306-X

DOI: 10.1016/j.tet.2017.03.057

Reference: TET 28563

To appear in: *Tetrahedron*

Received Date: 13 January 2017

Revised Date: 17 March 2017

Accepted Date: 21 March 2017

Please cite this article as: Yan J, Ni JC, Zhao JX, Sun LX, Bai FY, Shi Z, Xing YH, The nitro aromatic compounds detection by triazole carboxylic acid and its complex with the fluorescent property, *Tetrahedron* (2017), doi: 10.1016/j.tet.2017.03.057.

The Nitro aromatic compounds detection by triazole carboxylic acid and its complex with the fluorescent property

Jie Yan[a†], Jue Chen Ni[a†], Jin Xin Zhao[a], Li Xian Sun[b], Feng Ying Bai[a,*]

Zhan Shi[c] and Yong Heng Xing[a,*]

†These authors contributed equally.

[a]*College of Chemistry and Chemical Engineering, Liaoning Normal University, Dalian City, 116029, P.R. China*
[b]*Guangxi Key Laboratory of Information Materials, Guilin University of Electronic Technology, Guilin City, 541004, P.R. China*
[c]*State Key Laboratory of Inorganic Synthesis and Preparative Chemistry, College of Chemistry, Jilin University, Changchun City, 130012, P.R. China*
E-mail: xingyongheng2000@163.com
Tel: +86-411-82156987

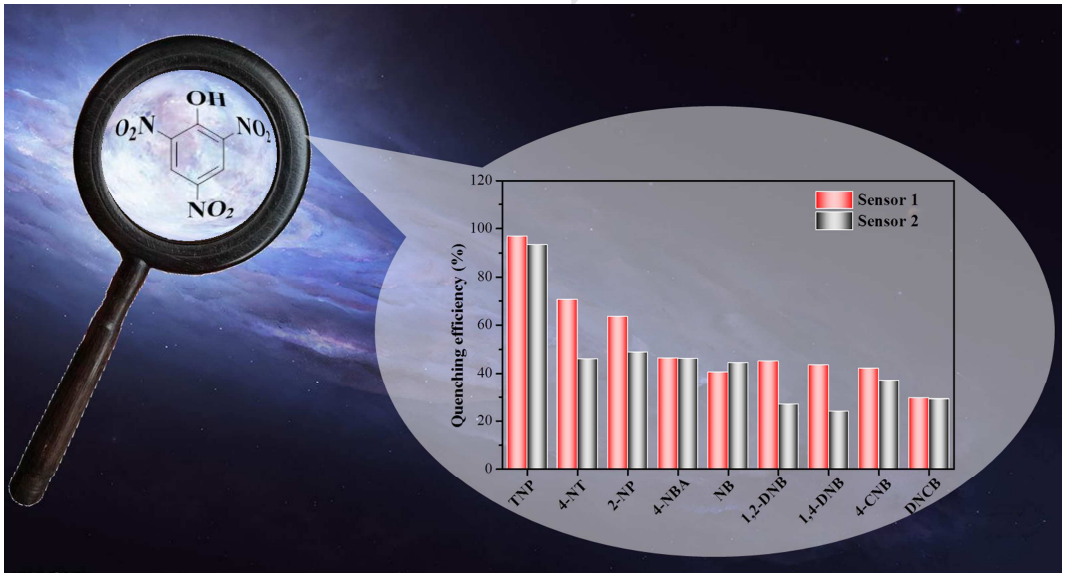

We firstly reported a triazole compound and its new complex as exclusive fluorescence sensor for TNP.

Graphical Abstract

The Nitro aromatic compounds detection by triazole carboxylic acid and its complex with the fluorescent property

We firstly reported a triazole compound and its new complex as exclusive fluorescence sensor for TNP.

Jie Yan[a†], Jue Chen Ni[a†], Jin Xin Zhao[a], Li Xian Sun[b], Feng Ying Bai[a,*] Zhan Shi[c] and Yong Heng Xing[a,*]
†These authors contributed equally.
[a]*College of Chemistry and Chemical Engineering, Liaoning Normal University, Dalian City, 116029, P.R. China*
[b]*Guangxi Key Laboratory of Information Materials, Guilin University of Electronic Technology, Guilin City, 541004, P.R. China*
[c]*State Key Laboratory of Inorganic Synthesis and Preparative Chemistry, College of Chemistry, Jilin University, Changchun City, 130012, P.R. China*

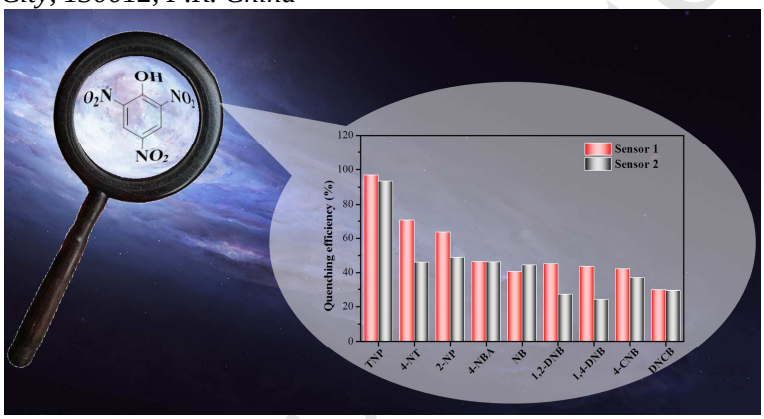

Tetrahedron
journal homepage: www.elsevier.com

The Nitro aromatic compounds detection by triazole carboxylic acid and its complex with the fluorescent property

Jie Yan[a†], Jue Chen Ni[a†], Jin Xin Zhao[a], Li Xian Sun[b], Feng Ying Bai[a]* Zhan Shi[c] and Yong Heng Xing[a1]*

†These authors contributed equally.

[a]*College of Chemistry and Chemical Engineering, Liaoning Normal University, Dalian City, 116029, P.R. China*
[b]*Guangxi Key Laboratory of Information Materials, Guilin University of Electronic Technology, Guilin City, 541004, P.R. China*
[c]*State Key Laboratory of Inorganic Synthesis and Preparative Chemistry, College of Chemistry, Jilin University, Changchun City, 130012, P.R. China*

ARTICLE INFO

Article history:
Received
Received in revised form
Accepted
Available online

Keywords:
Fluorescence sensor
Synthesis
Triazole
Nitro aromatic compounds
2, 4, 6-Trinitrophenol

ABSTRACT

The 5-methyl-1-(4-nitrophenyl)-1H-1, 2, 3-triazole-4-carboxylic acid (**1**) was synthesized by an improved method. By using the compound **1** as ligand, a new complex $[Cu(L)_2][Cu(L)_2(H_2O)_2]$ (**2**) was prepared firstly under hydrothermal condition. Both **1** and **2** were all used as exclusive fluorescence sensor for 2, 4, 6-trinitrophenol (TNP) for the first time. The fluorescence exploration demonstrated that they exhibit highly selective and sensitive (K_{SV} = 393685 M^{-1} and K_{SV} = 213269 M^{-1}, respectively) sensing to TNP from other nitro aromatic compounds (NACs) with high quenching efficiency QP value of 96.76% and 93.37%, as well as low detection limit (0.68μM and 0.37μM, respectively). It means that complex **2** had higher selectivity due to the less interference by 4-NT and 2-NP compared with **1**. Moreover, the fluorescence quenching phenomenon of sensor **1** with TNP was analyzed by density functional theory (DFT).

1. Introduction

Nitro aromatic compounds (NACs), in particular 2, 4, 6-trinitrophenol (TNP), are of great current concerns in both national security and environmental pollution because they are not only explosives but also recognized as toxic pollutants.[1] TNP is firstly synthesized as explosive used in militarily, which has strong explosion ability and low safety coefficient.[2] Its extensive appearance in the soil and ground water near military and industrial facilities may lead to serious environmental pollution.[3] Moreover, its ingestion can cause severe poisoning in humans, including headache, nausea, vomiting, abdominal pain and destruction of erythrocytes.[4] Thus, the sensing of TNP is highly essential for protecting personal safety and for controlling environmental pollution.[5] Recently, various techniques have been developed for the detection of TNP: mass spectrometry, ion mobility spectrometry, electrochemical methods, and colorimetry.[6] Compared with these analytical techniques, fluorescence-based detection offers several advantages such as high sensitivity, specificity and real-time monitoring with short response time.[7] Thereby, it is necessary to develop a rapid and sensitive fluorescence sensor to detect TNP.[8]

π- Conjugated heterocyclic compounds, such as oxadiazoles, thiadiazoles and triazoles constitute an important class of compounds in medicinal and pharmaceutical chemistry.[9] Among various π- conjugated heterocyclic compounds, triazoles have attracted attention in medicinal chemistry due to their numerous biological activities.[10] Triazoles are 5-membered rings, which contain two carbon and three nitrogen atoms.[11] According to the position of nitrogen atoms, the triazoles exist in two isomeric forms which are the 1, 2, 3-triazole and the 1, 2, 4-triazole.[12] In the past two decades, a large amount of drugs containing 1, 2, 3-triazole group such as Tazobactam, Cephalosporin and Cefatrizine have been synthesized.[13] They are clinically used for the treatment of bacterial infections.[14] In recent years, complexes containing metal Cu(Ⅱ) and 1,2,3-triazole ligands also have been extensively investigated.[15]

Until now, there have been lots of reports on the synthesis of 1, 2, 3-triazoles and 1, 2, 3-triazole complexes,[16] but less efforts have been made to use them as fluorescence sensor to detect TNP. In this paper, we improved the method of synthesizing 5-methyl-1-(4-nitrophenyl)-1H-1, 2, 3-triazole-4-carboxylic acid (**1**) and increased the yield (85%) in contrast to the previous literature (yield 67%). Then, we utilized compound **1** as a ligand to develop a new complex $[Cu(L)_2][Cu(L)_2(H_2O)_2]$ (**2**). To extend the functional properties of them, we show that compound **1** and complex **2** exhibit highly selective and low detection limit of 2, 4, 6-trinitrophenol (TNP), over other NACs such as nitrobenzene (NB), 4-nitrotoluene (4-NT), 4-nitrobenzaldehyde (4-NBA), 1,2-dinitrobenzene (1,2-DNB), 1,4-dinitrobenzene

Corresponding author Tel.: +86-411-82156987; E-mail: baifengying2000@163.com, xingyongheng2000@163.com; †: These authors contributed equally.

(1,4-DNB), 2-nitrophenol (2-NP), 2,4-dinitrochlorobenzene (DNCB), 4-chloronitrobenzene (4-CNB) via a "turn-off " fluorescence quenching in the dispersed state. In addition, the density functional theory (DFT) calculations also help us to understand the nature of interactions between compound **1** and TNP for its superior selectivity.

2. Results and discussion

*2.1. Synthesis of compound **1***

According to literature method, compound **1** and intermediate was synthesized in Scheme 1.[17] In the literature, aromatic azide was prepared from p-nitroaniline by diazotization reaction with sodium nitrite in HCl media acceding to sodium azide. Then, ethyl acetoacetate and the appropriate azide were slowly added together to the obtained MeOH/MeONa solution. 1, 3-dipolar cycloaddition was conducted by refluxing the aryl azide with ethyl acetoacetate under basic conditions for 1h using ethanol as solvent (67% yield). Based on plenty of experimental and data analysis, modified the order of the added was found as an efficient way to get higher yield. In this paper, ethyl acetoacetate was kept in the alkaline conditions for 30 minutes to make sure that the ethyl acetoacetate was deprotonated completely. Through the above-mentioned means, it could facilitate the formation of enol structure and 1, 3-dipolar cycloaddition would be reacted more fully with the aryl azide (yield increased to 85%). Meanwhile, X-ray single crystal structure (Fig. 1) of the compound **1** was firstly achieved.

*2.2. Structural description of complex **2***

X-ray single crystal study shows that complex **2** is crystallized in a monoclinic system with $P2_1/c$ space group. The structure of **2** comprises two moieties: $Cu(L)_2$ and $Cu(L)_2(H_2O)_2$, which are combined by electrostatic attraction and hydrogen bonds. The coordination environment of the copper atoms is shown in Fig. 2. Cu1(II) and Cu2(II) are both four-coordinated with a flat square geometry, but their coordination environments are different. Cu1(II) is coordinated by four oxygen atoms (O3, O3$^{\#}$ and O5, O5$^{\#}$; #: 2−x, -y, 1− z), which are from two compound **1** ligands and two coordinated water molecules, respectively; Cu2(II) is coordinated by two N atoms (N6, N6$^{\#}$; #: 2−x, -y, 1− z) and two oxygen atoms (O2, O2$^{\#}$; #: 2−x, -y, 1− z) from two **1** ligands. The bond length of Cu–N is 1.988(2) Å and those of Cu–O are in the range of 1.938(2)–1.963(2) Å. The angles of the O–Cu–O, O–Cu–N and N–Cu–N are in the range of 88.92(9)–180.0°, 82.66(9)–97.34(9)° and 180.0°, respectively. The dihedral angle between benzene rings (C5, C6, C7, C8, C9, C10; C11, C12, C14, C15, C16, C13) and the triazole rings (C2, C3, N3, N2, N1; C17, C19, N6, N5, N4) are 38.95 (0.08) ° and 54.62 (0.08) °, showing that C-N single bond distorting between benzene ring and the triazole ring is strong. For **1** ligand, it adopts a terminal monodentate coordination mode in Cu1 moiety and bidentate chelating coordination mode in Cu2 moiety, the bond length of Cu–N_L is 1.988(2) Å and the distance of Cu–O_L are 1.938(2) and 1.963(2) Å. In the packing structure of complex **2**, there are three kinds of hydrogen bonds: (i) hydrogen bond (O5–H5A···O2) between the oxygen (donor) from coordinated water molecule and the oxygen (acceptor) from **1** ligand; (ii) hydrogen bond (C–H···O) between the carbon (donor) and the oxygen (acceptor) from **1** ligand: C4–H4B···O4 and C18–H18C···O7; (iii) hydrogen bond (C13–H13···N1) between the carbon(donor) from benzene ring and the nitrogen (acceptor) from triazole ring. Through the hydrogen bond of O5–H5A··· O2, a 1D chain structure is formed. By the hydrogen bonding of C4–H4B···O4, the 1D chains are further connected to form a 2D supramolecular sheet structure.

2.3. Fluorescence sensing of nitro aromatic compounds

The emission spectra of the compound **1** and the complex **2** were shown in Fig. S9-S10 and the luminescent spectra of them were analyzed under excitation wavelength 320 nm and 300nm, respectively. The fluorescence quantum yield (Φ_F) of the compound **1** and the complex **2** were 0.068 and 0.047, respectively. Compound **1** and complex **2** are highly soluble in DMSO and the sensing study on them was carried out in V_{DMSO}: V_{H2O} =1:1. When small amount of 2, 4, 6-trinitrophenol (TNP) was added to the 10μM solution of them, the initial fluorescence intensity was quenched considerably, which inspired us to systematically establish the applicability of sensor **1** (compound **1**) and sensor **2** (complex **2**) for the detection of nitro aromatic compounds (NACs).

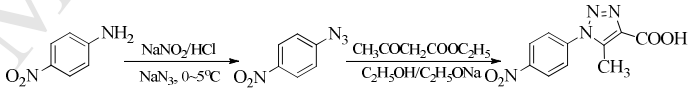

Scheme 1. Synthetic routes of compound **1**

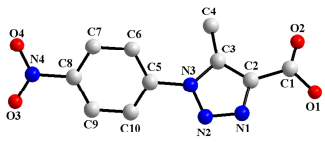

Figure 1. The crystal structure of compound **1**(hydrogen atoms and the lattice water molecule are omitted for clarity)

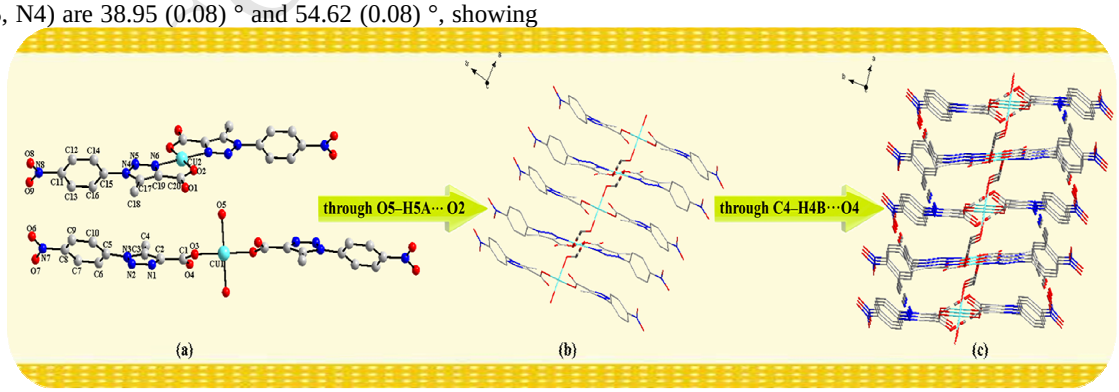

Figure 2. (a) The coordination environment of the Cu (II) ion in complex **2** (the hydrogen atoms have been omitted for clarity. Symmetry code: #1: -x+1,-y,-z+2; #2: -x+2,-y,-z+1). (b) The 1D chain structure of complex **2** along the a-axis (Symmetry code: #3: –x+2, –y, –z+2). (c) A view of the hydrogen bonds of complex **2** (part of the hydrogen atoms are omitted for clarity. Symmetry code: #3: –x+2, –y, –z+2; #4: 1-x, -y, 1-z; #5: x, y, -1+z; #6: 1+x, y, 1+z).

To gain a better understanding on the quenching efficiency and quenching rate (sensitivity) in the presence of NACs, fluorescence quenching titrations were performed by gradual addition of 1 or 2 ppm solution of several analytes to 10μM solution of the sensors. In the study, the NACs including 2,4,6-trinitrophenol (TNP), nitrobenzene (NB), 4-nitrotoluene (4-NT), 4-nitrobenzaldehyde (4-NBA), 1,2-dinitrobenzene (1,2-DNB), 1,4-dinitrobenzene (1,4-DNB), 2-nitrophenol (2-NP), 2,4-dinitrochlorobenzene (DNCB) and 4-chloronitrobenzene (4-CNB) are used to evaluate the quenching efficiency of sensing for nitro aromatic compounds. The representative titrations with TNP for sensors **1** and **2** are given in Fig. 3 and the titration with the other analytes are provided in the supporting information (Fig.S11-S12). In all cases, the initial fluorescence intensity of the sensors decreased dramatically upon gradual addition of the NACs. As shown in Fig. 4, the quenching percentage (QP = $(I_0 - I)/I_0 \times 100\%$, I_0 and I are luminescence intensity of sensor before and after exposure to the nitro compound) of sensor **1** was 96.76% for TNP, 70.44% for 4-NT, 63.44% for 2-NP, 46.36% for 4-NBA, 45.15% for 1, 2-DNB, 43.48% for 1, 4-DNB, 42.21% for 4-CNB, 40.56% for NB, 29.66% for DNCB. Correspondingly, the QP of sensor **2** was 93.37% for TNP, 48.79% for 2-NP, 46.28% for 4-NBA, 46.05% for 4-NT, 44.42% for NB, 37.15% for 4-CNB, 29.20 for DNCB, 27.08% for 1, 2-DNB, 24.00% for 1, 4-DNB. The experiments revealed that, both sensor **1** and **2** have significantly fluorescence quenching efficiency for the detection of TNP. Considering the interference by 4-NT and 2-NP, sensor **2** had better selectivity for the detection of TNP.

Furthermore, the sensitivity is evaluated through the Stern–Volmer equation ($I_0/I = K_{SV}[Q] + 1$), where K_{SV} is Stern–Volmer constants indicating the sensors sensitivity; I_0 and I are the fluorescence intensities before and after the addition of the analytes, [Q] is the concentration of the analytes. As shown in Fig. 5, all nitro analytes at low concentrations (up to 5 ppm) show linear proportional in (I_0/I-1). The SV plots began to bend upwards with the increase of the nitro analytes concentration, diverging from linearity (Fig. 6). The linear relationship at lower concentrations is mainly due to static quenching, whereas the deviation from linearity at higher concentrations is presumably due to dynamic quenching. The static quenching can be attributed to the ground state interaction between the analytes and the sensors. The dynamic quenching is mainly due to the energy and electron-transfer process between the analytes and sensors. Fitting of linear parts allows the quenching constants (K_{SV}) of sensor **1** to be 393685 M^{-1} for TNP, 28092 M^{-1} for 4-NT, 23077 M^{-1} for 2-NP, 15953 M^{-1} for 1,2-DNB, 13478 M^{-1} for 4-NBA, 12490 M^{-1} for 1,4-DNB, 9171 M^{-1} for NB, 8353 M^{-1} for 4-CNB, 7622 M^{-1} for DNCB and of sensor **2** to be 213269 M^{-1} for TNP, 16386 M^{-1} for 2-NP, 14808 M^{-1} for 4-NBA, 14587 M^{-1} for 4-NT, 13380 M^{-1} for 4-CNB, 10968 M^{-1} for NB, 9427 M^{-1} for DNCB, 8439 M^{-1} for 1,2-DNB, 5396 M^{-1} for 1,4-DNB, respectively. The larger K_{SV} values observed reveals high sensitivity, which made sensor **1** and **2** be the candidate of fluorescent sensor compounds for detection of TNP. The determination of the individual Stern-Volmer constants indicates that the fluorescence quenching mainly occurs through electron transfer. To further establish the formation of electron transfer, NMR titration of sensor **1** with TNP was performed. Sensor **1** was added into 5 ppm and 10 ppm solution of TNP in DMSO-d_6 that gives the NMR spectrum as shown in Fig. 7, significant chemical shifts of H_A and H_B protons for the sensor **1**, in addition to TNP, are observed in the ^1H NMR spectra (Table 1). The chemical shift of hydrogen protons on phenyl ring moves more prominently in comparison to other hydrogen protons. This observation suggests an electron transfer interaction between TNP and sensor **1**.

Enthused from these interesting outcomes, TNP selectivity in the presence of other nitro explosives was thoroughly checked. We studied the competing experiment in presence of other nitro analytes, of which DNCB was added initially to the V_{DMSO}: V_{H2O} =1:1 solution of sensor **1** and **2**, then, TNP and DNCB were alternately added. Similarly, the process was performed for other competing analytes. The experimental results show that DNCB merely lead to a minor fluorescent quenching effect, subsequent addition of TNP results in a strikingly prompt and noteworthy response for fluorescent quenching. The similar results are also observed for the other competing analytes, all of which have a similar plot (Fig. 8) of stepwise increase of quenching efficiency against the alternative addition of competing analytes and TNP. Consequently, high selectivity of sensor **1** and **2** for TNP is confirmed. For this result, we speculate that the high selectivity of sensor **1** and **2** for TNP was owing to the outstanding properties of triazole ligand. Besides, the selective experiments further support the conclusion of fluorescence quenching experiments that sensor **2** have higher selectivity due to the less interference by 4-NT and 2-NP than sensor **1**. The detection limit of the sensors for the TNP was calculated by following equation: detection limit = 3σ/k. Where, σ is the standard deviation of the blank measurement and k is the slope between the fluorescence intensity versus TNP concentration. The detection limit of the sensor **1** and sensor **2** are calculated to be 0.68 μM for TNP, 0.37 μM for TNP, respectively.[18]

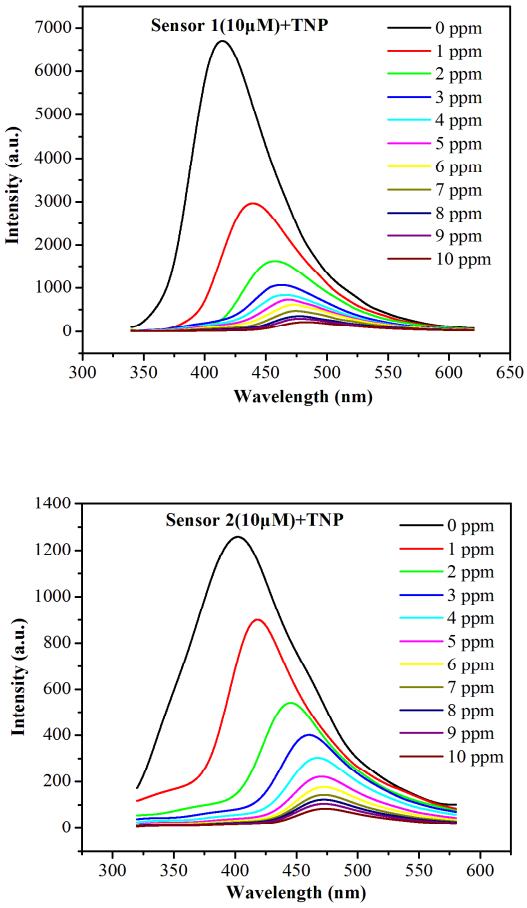

Figure 3. Reduction of the fluorescence emission intensity of the sensor **1** and **2** upon gradual addition of TNP (1-10 μl, 10^{-3} g/mL TNP were added to 3 mL sensor **1** and sensor **2** solution respectively).

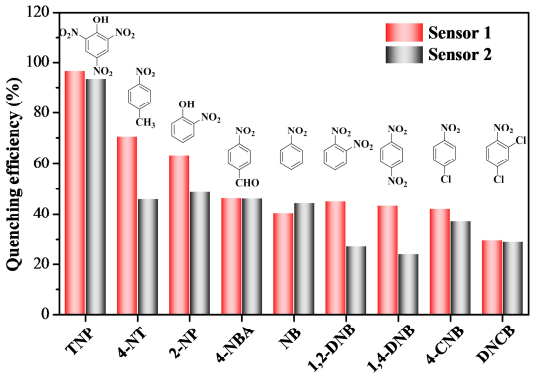

Figure 4. The column graph of reduction in fluorescence intensity (plotted as quenching efficiency) upon the addition of different analytes (10 µl, 10^{-3} g/mL NACs were added to 3 mL sensor **1** and sensor **2** solution respectively).

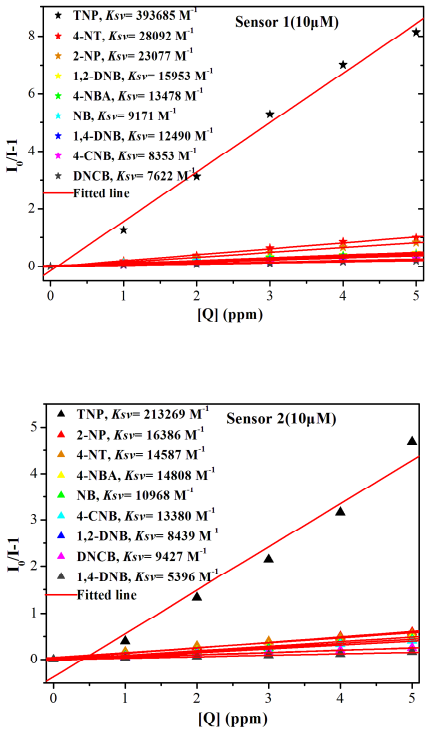

Figure 5. Stern–Volmer plots of analytes in lower concentration ranges of analytes (up to 5 ppm) (1-5 µl, 10^{-3} g/mL analytes were added to 3 mL sensor **1** and sensor **2** solution respectively).

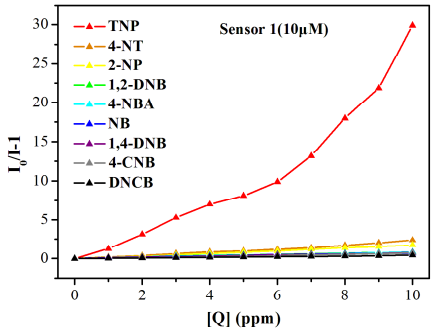

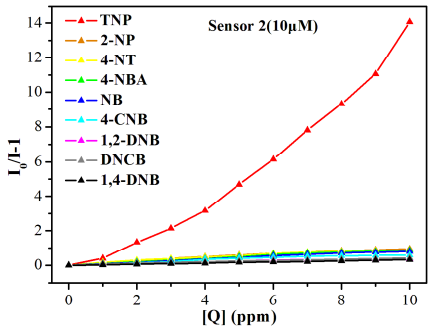

Figure 6. Stern–Volmer plots of analytes in higher concentration ranges of analytes (up to 10 ppm) (1-10 µl, 10^{-3} g/mL analytes were added to 3 mL sensor **1** and sensor **2** solution respectively).

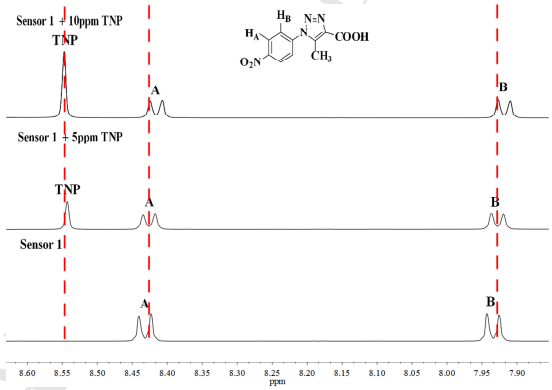

Figure 7. NMR with addition TNP to sensor **1** in DMSO-d_6 (5µl and 10 µl, 10^{-3} g/mL TNP were added to 3 mL sensor **1** solution respectively).

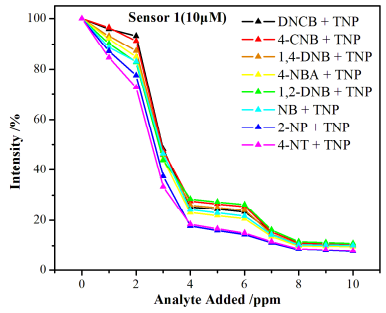

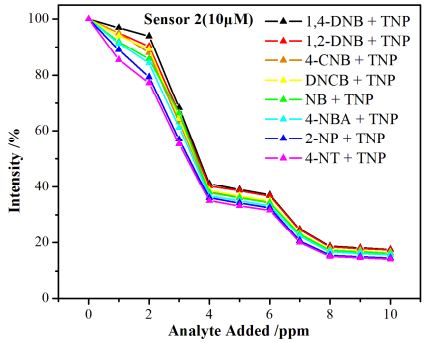

Figure 8. Fluorescence quenching of sensor **1** and **2** upon addition of DMSO/H_2O solutions of different nitro compounds followed by TNP (1-10 µl, 10^{-3} g/mL different NACs and TNP were alternately added to 3 mL sensor **1** and sensor **2** solution respectively).

Table 1. The NMR chemical shifts of sensor **1** with TNP in DMSO-d_6

Chemical shift	TNP/ppm	H_A/ppm		H_B/ppm	
Sensor **1**	-	8.440	8.423	7.943	7.926
Sensor **1** +5ppm TNP	8.543	8.434	8.417	7.936	7.919
Sensor **1** +10ppm TNP	8.547	8.424	8.407	7.927	7.910

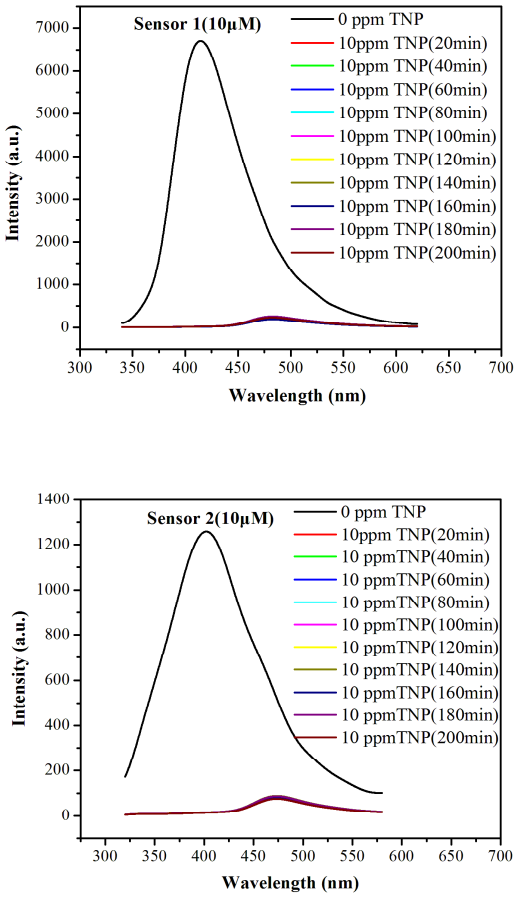

Figure 9. Photo stability test: Fluorescence spectra of sensor **1** and sensor **2** in presence of 10 ppm of TNP at different time scale (10 μl, 10^{-3} g/mL TNP were added to 3 mL sensor **1** and sensor **2** solution respectively).

In addition to the sensitivity and selectivity for TNP, the photo stability required for sensing is also very significant for practical application. The fluorescence response of TNP is quick quenching process. Typically, the inorganic and organic fluorophore does not have any photo stability that leads to fluorescence activity changes with time. The quenching fluorescence intensity in presence of TNP does not show any change in fluorescence spectrum with temporal variation as demonstrated in Fig. 9. The present sensors for TNP detection are comparable or superior to the methods reported earlier.[19]

2.4. Mechanism for detection of TNP

The fluorescence quenching phenomenon can be described by a donor–acceptor electron transfer mechanism between the sensor and TNP.[20] One can anticipate that the electron transfer could take place upon excitation if the LUMO of the electron deficient analytes resides in between the HOMO and the LUMO of the sensors. Upon excitation of the sensor, a charge transfer takes place from the LUMO of the sensor to the LUMO of TNP, thus, resulting in initial fluorescence quenching. Estimation of the HOMO and LUMO energy of the sensor as well as for TNP by density functional theory (DFT) revealed that the LUMO of the electron deficient TNP is situated in between the HOMO and LUMO of the sensor. Hence, an excited-state electron transfer is expected from the LUMO of the sensor to TNP. The difference in the energy between the LUMO of the sensor and TNP implicate that TNP has good fluorescence quenching ability. In addition, to support the experimental charge-transfer mechanism between the sensor and TNP, a series of computational calculations was carried out employing DFT. The geometry optimization of the sensor in the presence of TNP revealed that the most favorable location (in terms of energy) for TNP interacting with the sensor was related to the carboxyl of triazole ring moiety. If TNP formed a charge-transfer complex with the sensor, the LUMO of the newly formed complex should be lower in energy compared to the sensor itself. However, the energy level of HOMO kept almost the same comparing to that of the sensor. In Fig. 10, a representative energy diagram of sensor **1**, TNP and [sensor **1** +TNP] indicated that the initial HOMO and LUMO energy difference of sensor **1** (4.57 eV) is reduced to 3.61 eV in the presence of TNP. In this process, the energy of the LUMO of sensor **1** (-2.92 eV) decreases firmly by 0.91 eV to the newly formed LUMO (-3.83 eV) of the [sensor **1** +TNP] adduct, however, the HOMO energy does not change significantly. To our expectation, the LUMO of [sensor **1** +TNP] has the contribution mainly on the TNP moiety and the HOMO is located on the carboxyl of triazole ring moiety of sensor **1**.

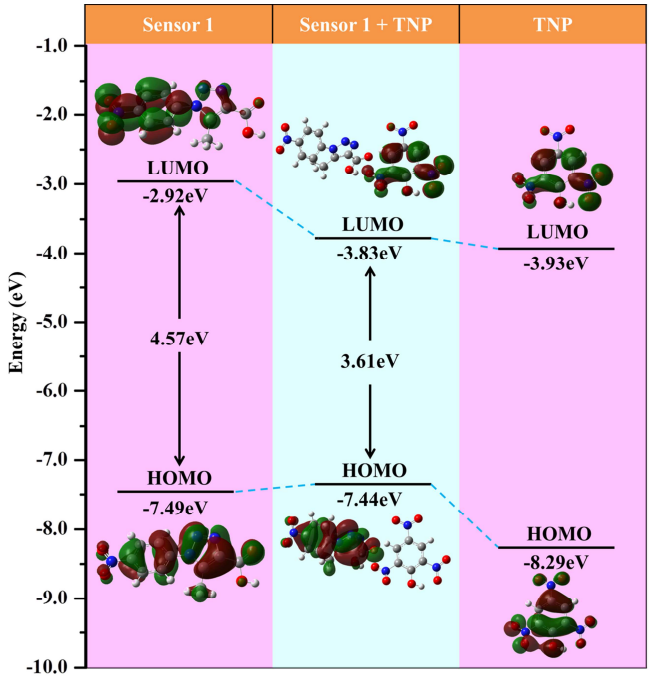

Figure 10. Calculated energy level diagram of sensor **1**, TNP and [sensor **1** + TNP]

3. Conclusions

In summary, aiming at developing and enriching inorganic and organic fluorescent materials, we prepared a triazole derivative with carboxylic acid group (compound **1**) by modified method and utilized it as a ligand to develop a new metal copper complex (complex **2**). Compound **1** was characterized by elemental analysis, ^{1}H NMR and ^{13}C NMR. Correspondingly, Complex **2** was characterized by spectroscopy elemental analysis, IR, UV–vis spectroscopy and powder X-ray diffraction (PXRD). Both of them showed high sensitivity, selectivity and low detection limit for TNP. Then we had a discussion about the fluorescence quenching mechanism of the sensor **1** (compound **1**) with TNP based on the density functional theory (DFT) calculations. Therefore, the syntheses of this kind of compounds were very successful, whose potential applications in inorganic and organic fluorescent materials were widespread and valuable.

4. Experimental section

4.1. Materials and methods

Compound **1** was synthesized according to the modified literature method.[17] All other chemicals were purchased from commercial sources and used as received. Solvents were dried and distilled prior to use by standard procedure. IR spectra were recorded on a Bruker AXS TENSOR-27 FT-IR spectrometer with pressed KBr pellets in the range of 4000-400 cm^{-1}. ^{1}H NMR and ^{13}C NMR were recorded in DMSO-d_6 on a Bruker AV 500 O FT-NMR spectrometer operating at 500 and 125 MHz, respectively. The high resolution mass spectrum was recorded with an Agilent 6540. The elemental analyses for C, H, and N were carried out on a Perkin Elmer 240C automatic analyzer. UV-vis absorption spectra were recorded with a JASCO V-570 UV/VIS/NIR spectrophotometer in the range of 200-2500 nm. X-ray powder diffraction (PXRD) patterns were obtained on a Bruker Advance-D8 equipped with Cu Kα radiation, in the range of 5° < 2θ < 60°, with a step size of 0.02° (2θ) and a count time of 2 s per step. Fluorescence emission studies were carried out on Hitachi F-7000 fluorescence spectrophotometer. For this experiment, a 10^{-5}M solution of the individual sensor was prepared in DMSO/H_2O (1:1) and subsequently 3 mL solution was placed in quartz cuvette. The geometries of all compounds were optimized by density functional (DFT) methods by using the Gaussian 09 program. For optimization, B3LYP functional was used employing 631G* basis set.

4.2. Synthesis

5-Methyl-1-(4-nitrophenyl)-1H-1, 2, 3-triazole-4-carboxylic acid (**1**): Sodium nitrite (3.45 g, 0.05mol) in cold distilled water (15 mL) was slowly added to the p-nitroaniline (6.91g, 0.05mol) in concentrated hydrochloric acid (25 mL) at 0^{o}C with stirring for 50 minutes. Then, the mixture was stirred around 0^{o}C (no more than 5^{o}C) for 30 minutes. After filtration, sodium azide (3.25 g, 0.05mol) dissolved in distilled water (10 mL) was added to the solution. The solution was stirred at room temperature for 2 h. The white solid was collected by filter. Metallic sodium (0.5 g, 0.02mol) was added to cold absolute ethanol (10mL). After the reaction was completely finished, ethyl acetoacetate (1.31 g, 0.01mol) was added dropwise into mixture at 0^{o}C with stirring. When the system was reacted for 30 minutes, the organic azide (1.63 g, 0.01mol) was added to mixture with stirring in the ice water bath. The mixture was heated to the boiling point slowly and kept the temperature at the boiling point for 1 hour. Hot water was added to the solution until the precipitation disappeared. The mixture was kept heating for 10 minutes and then cooled to room temperature. The resulting solution was acidified with 2M HCl. The crude product was recrystallized in ethanol to give compound **1** as white solid (2.10 g, 85%). Anal. Calc. for $C_{10}H_8N_4O_4$ (248.19): C, 48.67; H, 3.29; N, 22.46%. Found: C, 48.39; H, 3.25; N, 22.57%. IR data (KBr, cm^{-1}): 3480, 3125, 2866, 1714, 1580, 1513, 1445, 1346, 1268, 1228, 1114. ^{1}H NMR (500 MHz, DMSO-d_6): δ (ppm) 13.19 (s, 1H), 8.44-8.42 (d, J = 8.6 Hz, 2H), 7.94-7.93 (d, J = 8.6 Hz, 2H), 2.54 (s, 3H). ^{13}C NMR (125 MHz, DMSO-d_6): δ (ppm) 162.82, 148.32, 140.56, 139.94, 137.46, 126.96, 125.51, 10.25. HRMS (ESI): m/z calcd for $C_{10}H_8N_4O_4$ $[M+H]^+$ 249.0625, found 249.0624.

Table 2. Crystallographic data and the structure refinement for compound **1** and complex **2***

Compound/Complex	**1**	**2**
Formula	$C_{10}H_{10}N_4O_5$	$C_{40}H_{32}N_{16}O_{18}Cu_2$
M (g·mol^{-1})	266.22	1151.90
Crystal system	Monoclinic	Monoclinic
Space group	*P*2(1)/*n*	$P2_1/c$
a (Å)	11.656(2)	7.7352(9)
b (Å)	7.7162(16)	35.847(4)
c (Å)	14.086(3)	8.4927(10)
α (°)	90	90
β (°)	108.360(4)	108.903(2)
γ (°)	90	90
V (Å^3)	1202.4(4)	2227.9(4)
Z	4	2
D_{calc} (g·cm^{-3})	1.471	1.717
Crystal size (mm)	0.41 x 0.22 x 0.19	0.40 x 0.35 x 0.31
F(000)	552	1172
μ(Mo-Kα) mm^{-1}	0.120	1.054
Reflections collected	7527	13549
Independent reflections	2933	5149
Parameters	174	348
Δ(ρ) (e Å^{-3})	0.269, -0.262	0.470, -0.668
Goodness of fit	1.012	1.048
R^a (R^b)	0.0553 (0.1138)	0.0456 (0.0784)
wR_2^{a} (wR_2^{b})	0.1237 (0.1468)	0.1200 (0.1417)

*[a] $R = \Sigma||F_o| - |F_c||/\Sigma|F_o|$, $wR_2 = [\Sigma(w(F_o^2 - F_o^2)^2/\Sigma(w(F_o^2)^2)]^{1/2}$; $[F_o > 4\sigma(F_o)]$. [b] Based on all data.

Table 3. The detailed attribution of IR (cm^{-1}) for compound **1** and complex **2**

Compound/ Complex	**1**	**2**
$\nu_{(O-H)}$	3480	3443
$\nu_{(Ar-H)}$	3125	3085
$\nu_{(CH3)}$	2866	2864
$\nu_{(C=O)}$	1714	-
$\nu_{as(COO^-)}$	-	1636
$\nu_{s(COO^-)}$	-	1434
$\nu_{(phenyl)}$	1580, 1445	1617
$\nu_{(triazole)}$	1346, 1228, 1114	1348, 1252, 1127
$\nu_{as(NO2)}$	1513	1521
$\nu_{s(NO2)}$	1268	1300

$[Cu(L)_2][Cu(L)_2(H_2O)_2]$ (**2**): $CuCl_2 \cdot 2H_2O$ (0.017 g, 0.10 mmol) and compound **1** (0.025 g, 0.10 mmol) were mixed in a beaker with the mixture of water (10 mL) and EtOH (5 mL) then stirred for 3 h. The final reaction mixture was sealed in a 25 mL Teflon-lined stainless steel vessel under autogenous pressure and heated at 160 °C for 4 days, and then followed by slow cooling to room temperature. After filtration, the product was washed with distilled water and then dried at room temperature. Some blue crystals suitable for X-ray diffraction analysis were obtained. Yield: 32% (based on Cu). Anal. Calc. for $C_{40}H_{32}N_{16}O_{18}Cu_2$ (1151.90): C, 41.71; H, 2.80; N, 19.46%. Found: C, 41.70; H, 2.85; N, 19.42%. IR data (KBr, cm^{-1}): 3443, 3085, 2864, 1636, 1617, 1521, 1434, 1348, 1300, 1252, 1127.

4.3. X-ray crystallographic determination

Suitable single crystals of the compound **1** and complex **2** were mounted on glass fibers for X-ray measurement, respectively. Reflection data were collected at room temperature on a Bruker AXS SMART APEX Ⅱ CCD diffractometer with graphite monochromatized Mo Kα radiation (λ = 0.71073 Å). All absorption corrections were performed using the SADABS program. Crystal structures were solved by the direct method. All non-hydrogen atoms were refined anisotropically. All hydrogen atoms were fixed at calculated positions with isotropic thermal parameters except for the coordinated water molecules, which were located by difference Fourier map. All calculations were performed using the SHELX-97 program. Crystal data and details of the data collection and the structure refinement of compound **1** and complex **2** are given in Table 2. For compound **1** and complex **2**, the selected bond lengths and bond angles are listed in Table S1; the hydrogen bonds of complex **2** are shown in Table S2. The drawings were made with Diamond 3.2.

4.4. IR spectra

The IR spectra of compound **1** and complex **2** are examined (Fig.S4-S5). For compound **1**, a broad absorption band appearing at 3480 cm^{-1} can be attributed to the O–H stretching vibrations of the carboxyl group. Absorption band at 3125 cm^{-1} should be assigned to the stretching vibrations of the =C–H in the phenyl ring. Weak absorption band observed at 2866 cm^{-1} is features of the ν_{C-H} vibration modes of $-CH_3$ group. Strong Absorption at 1714 cm^{-1} is the characteristic stretching vibration of the $\nu_{C=O}$ bond. The bands at 1580, 1445, 1346, 1228, and 1114 cm^{-1} are attributed to the characteristic stretching vibrations of the phenyl and triazole rings. The peaks at 1513 and 1268 cm^{-1} are the characteristic absorptions for the asymmetric and symmetric stretching vibrations of $-NO_2$ group, respectively. Because the stretching vibrations of $-NO_2$ group and the characteristic stretching vibrations of the phenyl and triazole rings both appear at 1600-1200 cm^{-1}, and overlap partially, the absorption bands in this region are comparatively broad. IR spectral characteristic of complex **2** is similar to compound **1**, except the peaks at 1636 and 1434 cm^{-1} are the characteristic absorptions for the asymmetric and symmetric stretching vibrations of the carboxylate group in the triazole ligand. The detailed appointments of the IR spectra data for compound **1** and complex **2** are listed in Table 3.

Table 4. The detailed attribution of UV-vis (nm) for compound **1** and complex **2**

Compound/ Complex	**1**	**2**
π–π*/ n–π*	217, 260, 306	219, 262, 339
LMCT	-	415
d–d*	-	720 $^2E_g \rightarrow {}^2T_{2g}$

4.5. UV-vis spectra

The electronic absorption spectra of compound **1** and complex **2** were recorded at room temperature in the form of a solid sample. As shown in Fig. S6–S7, electronic absorption spectra of compound **1** and complex **2** have similar absorption patterns. There are three sharp and strong high-energy absorption bands in the region of 200-350 nm. Bands at 217, 260, 306 nm for compound **1** and 219, 262, 339 nm for complex **2** could be ascribed to n–π* or π–π* transition. The peak observed at 415 nm for complex **2** is attributed to the charge transitions from the ligand to the Cu (II) atoms (LMCT). The absorption band at 720 of complex **2** is caused by the d-d* transition of Cu^{2+}. Compared with compound **1**, it is found that complex **2** shows slight red shifts about the high-energy absorption bands, indicating that the N-heterocyclic ligand of compound **1** was coordinated to metal center. The detailed appointments of the UV-vis spectra data for compound **1** and complex **2** are listed in Table 4.

4.6. PXRD analysis

The PXRD pattern of complex **2** is shown in Fig. S8. All the peaks presented in the measured patterns closely match the simulated patterns generated from the single crystal diffraction data, which indicate that the complex is phase pure.

Acknowledgments

This work was supported by the grants of the National Natural Science Foundation of China (Nos. 21571091, 21371086), State Key Laboratory of Inorganic Synthesis and Preparative Chemistry, College of Chemistry, Jilin University, Changchun 130012, P.R. China (No. 2016-02) and Guangxi Key Laboratory of Information Materials, Guilin University of Electronic Technology, P. R. China (Project No. 151002-K) for financial assistance for financial assistance. Furthermore, we also give thanks to the High-Performance Computing Platform of Guangxi University for generous support of our computational chemistry research.

References

1. (a) Pinrat, O.; Boonkitpatarakul, K.; Paisuwan, W.; Sukwattanasinitt, M.; Ajavakom, A. *Analyst* **2015**, *140*, 1886 - 1893; (b) Singha D. K.; Mahata P. *RSC Advances* **2015**, *5*, 28092 - 28097; (c) Dey, N.; Samanta S. K.; Bhattacharya S. *ACS Appl. Mater. Interfaces* **2013**, *5*, 8394 - 8400; (d) Li, X. G.; Liao, Y.; Huang, M. R.; Strong, V.; Kaner, R. B. *Chem. Sci.* **2013**, *4*, 1970 - 1978.
2. (a) Salinas, Y.; Martínez-Máñez, R.; Marcos, M. D.; Sancenón, F.; Costero, A. M.; Parra, M.; Gil, S. *Chem. Soc. Rev.* **2012**, *41*, 1261 - 1296; (b) Joarder, B.; Desai, A. V.; Samanta, P.; Mukherjee, S.; Ghosh, S. K. *Chem. Eur. J* **2015**, *21*, 965 - 969.

3. (a) Ma, D.; Li, B., Zhou, X.; Zhou, Q.; Liu, K.; Zeng, G.; Li, G.; Shi, Z.; Feng, S. *Chem. Commun.* **2013**, *49*, 8964 - 8966; (b) Zhao, L.; Ye, J.; Li, W.; Bogale, R. F.; Wang, B.; Gong, W.; Ning, G. *Inorg. Chem. Commun.* **2014**, *46*, 212 - 215.
4. (a) Mukherjee, S.; Desai, A. V.; Manna, B.; Inamdar, A. I.; Ghosh, S. K. *Cryst. Growth Des.* **2015**, *15*, 4627 - 4634; (b) Ma, H.; He, C.; Li, X.; Ablikim, O.; Zhang, S.; Zhang, M. *Sens. and Actuator B* **2016**, *230*, 746 - 752.
5. (a) Das, G.; Biswal, B. P.; Kandambeth, S.; Venkatesh, V.; Kaur, G.; Addicoat, M.; Heine, T.; Verma, S.; Banerjee, R. *Chem. Sci.* **2015**, *6*, 3931 - 3939; (b) Lin, L.; Rong, M.; Lu, S.; Song, X.; Zhong, Y.; Yan, J.; Wang, Y.; Chen, X. *Nanoscale* **2015**, *7*, 1872 - 1878; (c) Zhang, F.; Luo, L.; Sun, Y.; Miao, F.; Bi, J.; Tan, S.; Tian, D.; Li, H. *Tetrahedron* **2013**, *69*, 9886 - 9889.
6. (a) Bader, M.; Göen, T.; Müller, J.; Angerer, J. *J. Chromatogr. B* **1998**, *710*, 91 - 99; (b) Khayamian T.; Tabrizchi M.; Jafari M. T. *Talanta* **2003**, *59*, 327 - 333; (c) Naal, Z.; Park, J. H.; Bernhard, S.; Shapleigh, J. P.; Batt, C. A.; Abruna, H. D. *Anal. Chem.* **2002**, *74*, 140 - 148; (d) Hilmi, A.; Luong, J. H. *Anal. Chem.* **2000**, *72*, 4677 - 4682; (e) Peng, Y.; Zhang, A. J.; Dong, M.; Wang, Y. W. *Chem. Commun.* **2011**, *47*, 4505 - 4507.
7. (a) Liu, T.; Ding, L.; Zhao, K.; Wang, W.; Fang, Y. J. *Mater. Chem.* **2012**, *22*, 1069 - 1077; (b) Roy, B.; Bar, A. K.; Gole, B.; Mukherjee, P. S. *J. Org. Chem.* **2013**, *78*, 1306 - 1310; (c) Liu, T.; Zhao, K.; Liu, K.; Ding, L.; Yin, S.; Fang, Y. *J. Hazard. Mater.* **2013**, *246*, 52 - 60; (d) Liu, K.; Liu, T.; Chen, X.; Sun, X.; Fang, Y. *ACS Appl. Mater. Interfaces* **2013**, *5*, 9830 - 9836.
8. (a) Huynh, T. P.; Wojnarowicz, A.; Kelm, A.; Woznicki, P.; Borowicz, P.; Majka, A.; D'Souza, F.; Kutner, W. *ACS Sens.* **2016**, *1*, 636 - 639; (b) Ni, J. C.; Yan, J.; Zhang, L. J.; Shang, D.; Du, N.; Li, S.; Zhao, J. X.; Wang, Y.; Xing, Y. H. *Tetrahedron Lett.* **2016**, *57*, 4978 - 4982.
9. Yadagiri, B.; Gurrala, S.; Bantu, R.; Nagarapu, L.; Polepalli, S.; Srujana, G.; Jain, N. *Bioorg. Med. Chem. Lett.* **2015**, *25*, 2220 - 2224.
10. Koparir, M.; Orek, C.; Parlak, A. E.; Söylemez, A.; Koparir, P.; Karatepe, M.; Dastan, S. D. *Eur. J. Med. Chem.* **2013**, *63*, 340 - 346.
11. (a) Maier, G.; Eckwert, J.; Bothur, A.; Reisenauer, H. P.; Schmidt, C. *Liebigs Ann.* **1996**, *1996*, 1041 - 1053; (b) Guirado, A.; López-Caracena, L.; López-Sánchez, J. I.; Sandoval, J.; Vera, M.; Bautista, D.; Gálvez, J. *Tetrahedron* **2016**, *72*, 8055 - 8060.
12. Küçükgüzel, Ş. G.; Çıkla-Süzgün, P. *Eur. J. Med. Chem.* **2015**, *97*, 830 - 870.
13. Gomi, H.; Solomkin, J. S.; Takada, T.; Strasberg, S. M.; Pitt, H. A.; Yoshida, M.; Kusachi, S.; Mayumi, T.; Miura, F.; Kiriyama, S.; Yokoe, M.; Kimura, Y.; Higuchi, R.; Windsor, J. A.; Dervenis, C.; Liau, K. H.; Kim, M. H. *J. Hepatobiliary Pancreat Sci.* **2013**, *20*, 60 - 70.
14. Kant, R.; Kumar, D.; Agarwal, D.; Gupta, R. D.; Tilak, R.; Awasthi, S. K.; Agarwal, A. *Eur. J. Med. Chem.* **2016**, *113*, 34 - 49.
15. Li, J.; Xi, T.; Yan, B.; Guan, Y.; Yang, M.; Song, J.; Ma, H. *New J. Chem.* **2015**, *39*, 9550 - 9556.
16. (a) Ghosh, D.; Rhodes, S.; Hawkins, K.; Winder, D.; Atkinson, A.; Ming, W.; Padgett, C.; Orvis, J.; Aiken, K.; Landge, S. *New J. Chem.* **2015**, *39*, 295 - 303; (b) Chen, J. L.; Guo, Z. H.; Luo, Y. S.; Qiu, L.; He, L. H.; Liu, S. J.; Wen, H. R.; Wang, J. Y. *New J. Chem.* **2016**, *40*, 5325 - 5332.
17. (a) Benbayer, C.; Kheddam, N.; Saïdi-Besbes, S.; de Givenchy, E. T.; Guittard, F.; Grelet, E.; Safer, A. M.; Derdour, A. *J. Mol. Struct* **2013**, *1034*, 22 - 28; (b) Pokhodylo, N. T.; Teslenko, Y. O.; Matiyuchuk, V. S.; Obushak, M. D. *ChemInform* **2010**, *41*, 2741 - 2748.
18. Ding, B.; Liu, S. X.; Cheng, Y.; Guo, C.; Wu, X. X.; Guo, J. H.; Liu, Y. Y.; Li, Y. *Inorg. Chem.* **2016**, *55*, 4391 - 4402.
19. Muthu, C.; Nagamma, S. R.; Nair, V. C. *RSC Advances* **2014**, *4*, 55908 - 55911.
20. Gole, B.; Song, W.; Lackinger, M.; Mukherjee, P. S. *Chem. Eur. J* **2014**, *20*, 13662 - 13680.

Supplementary Material

Figures of ^{1}H NMR, ^{13}C NMR, IR spectra, UV-vis spectra, PXRD, fluorescence spectra and tables of crystal data are presented in the supplementary material. CCDC 1511387 for compound **1**, CCDC 1511372 for complex **2**.

Click here to remove instruction text...

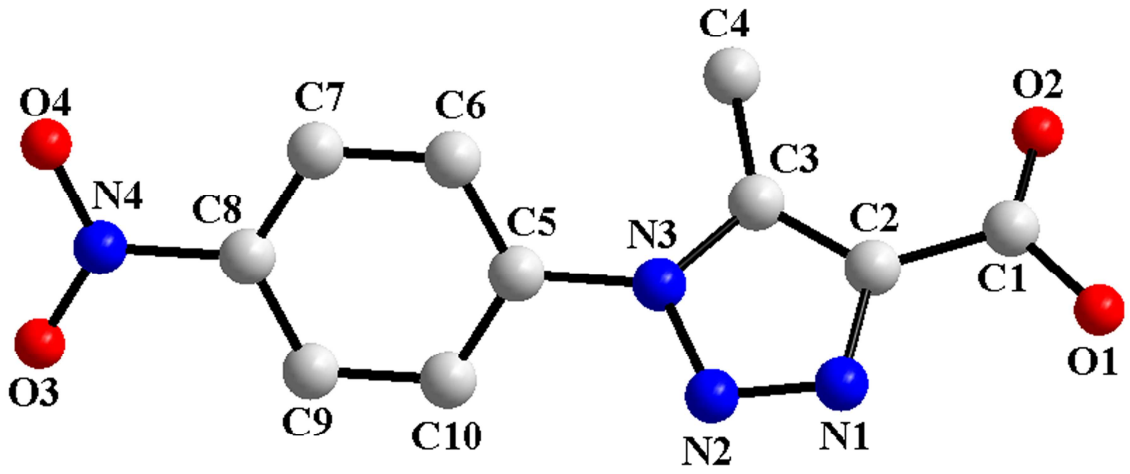

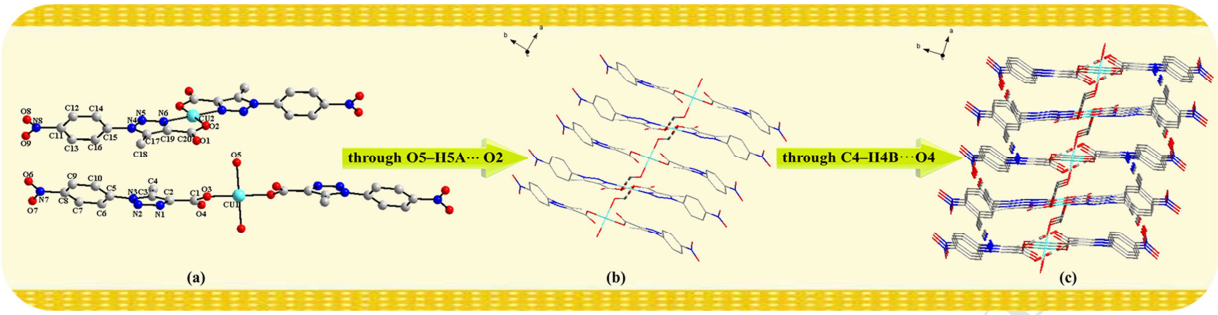

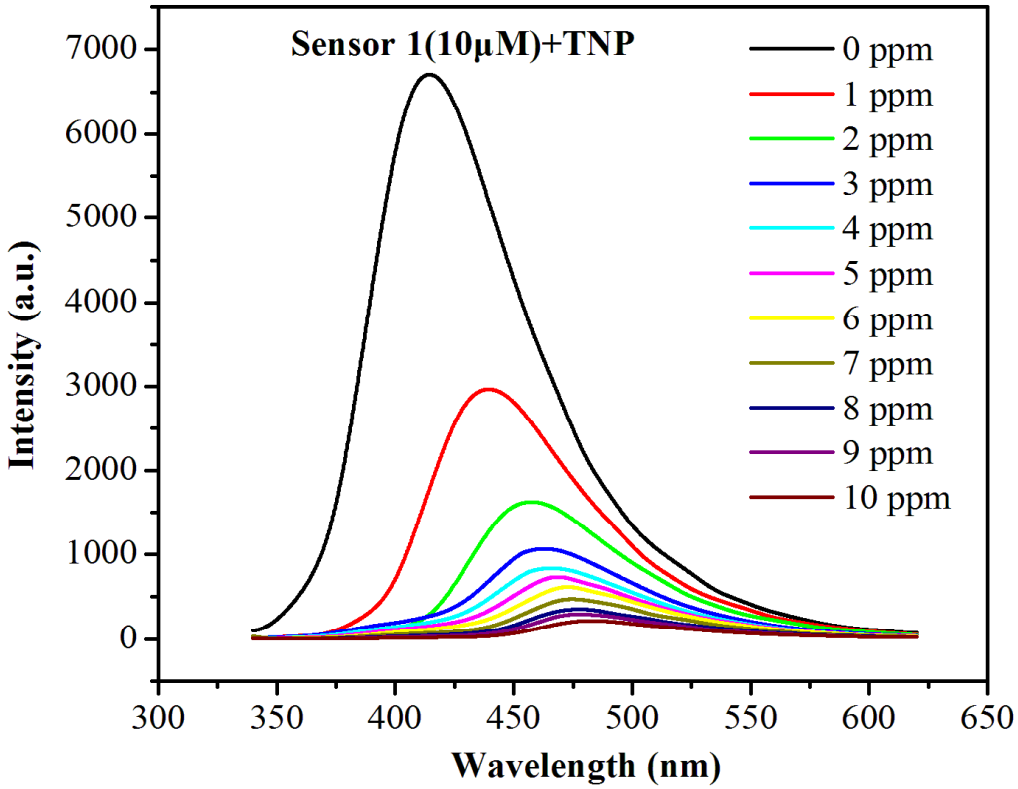

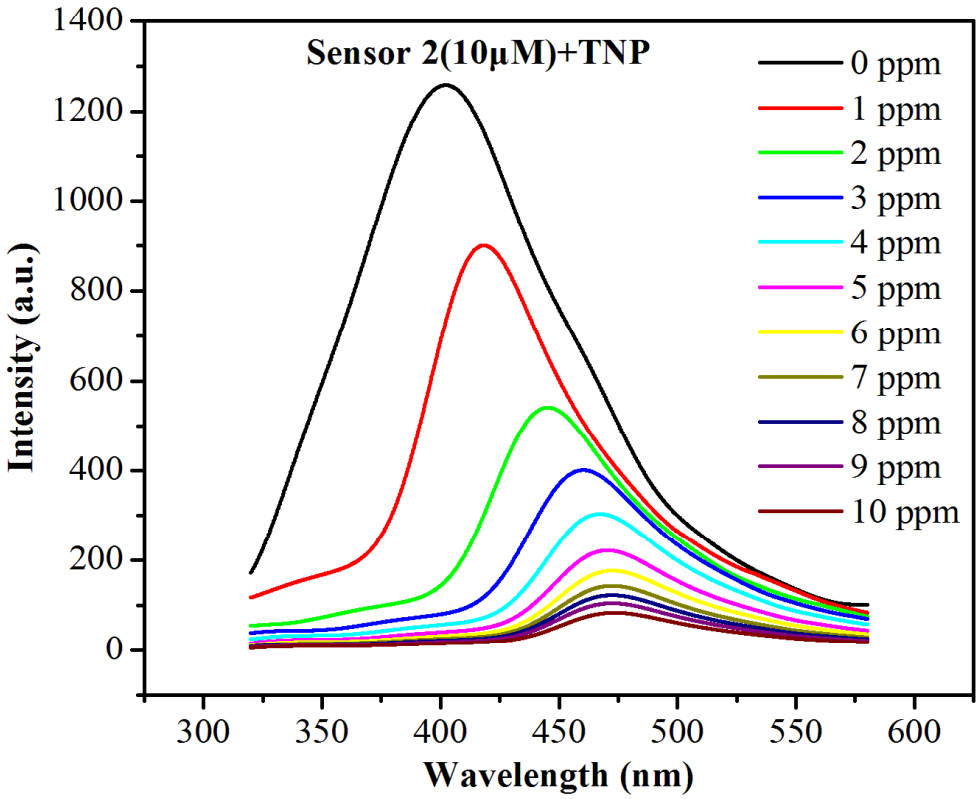

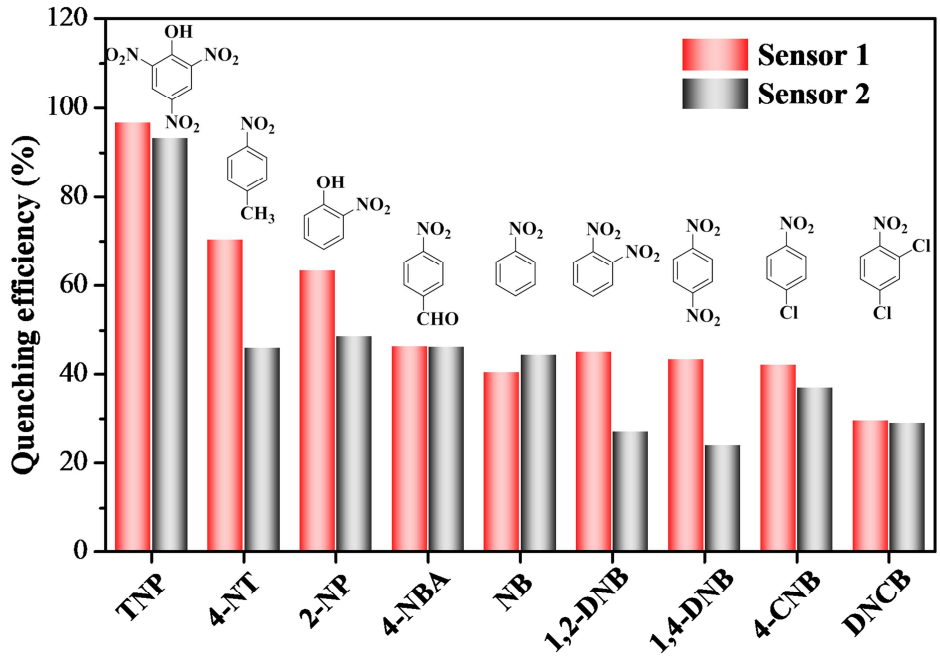

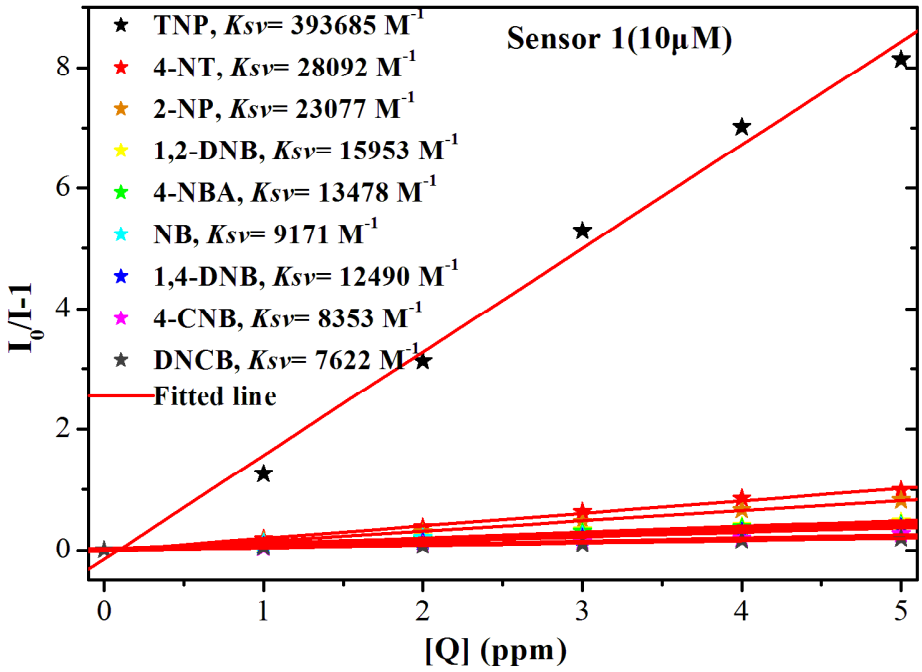

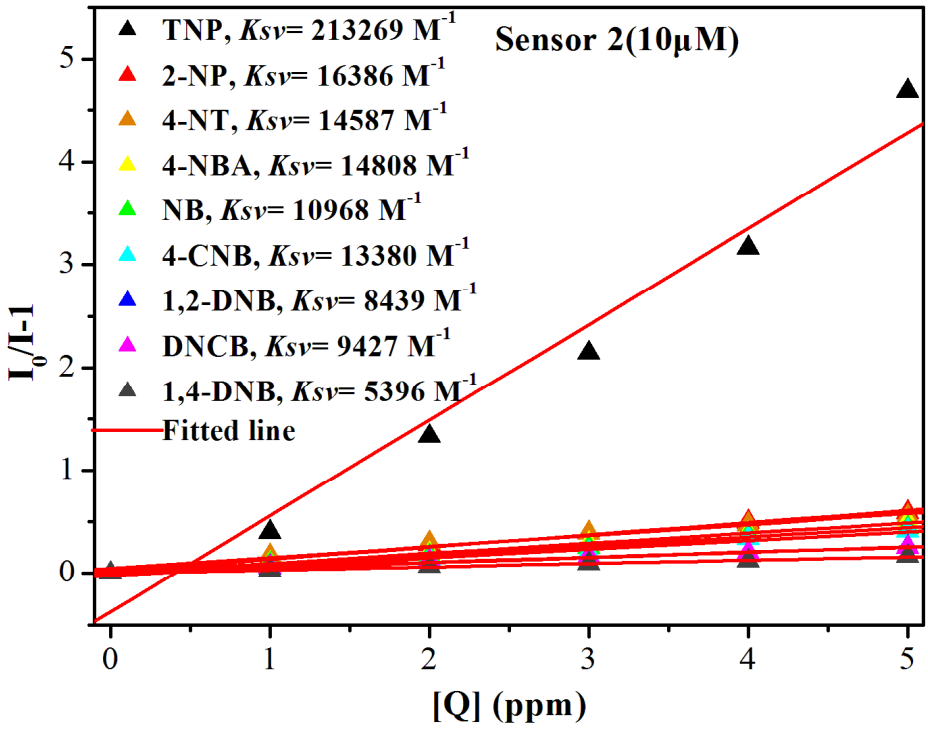

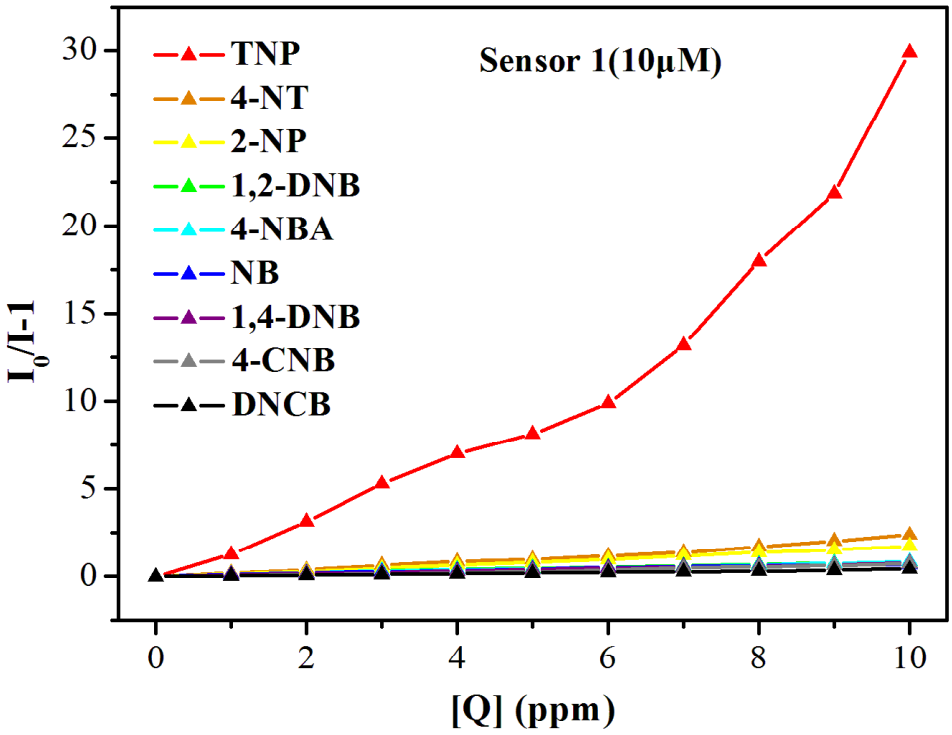

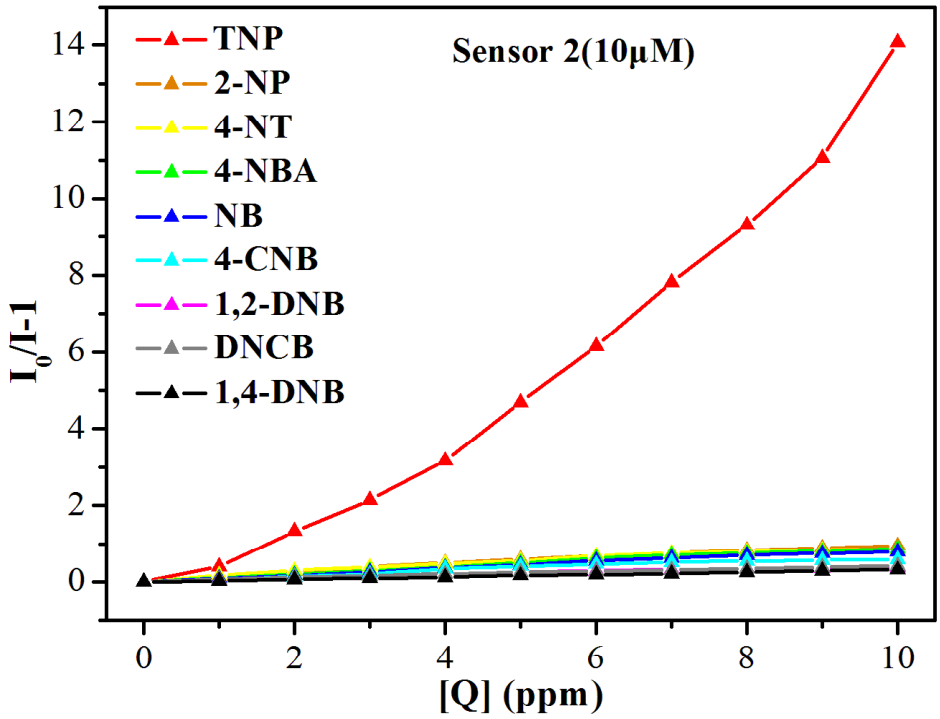

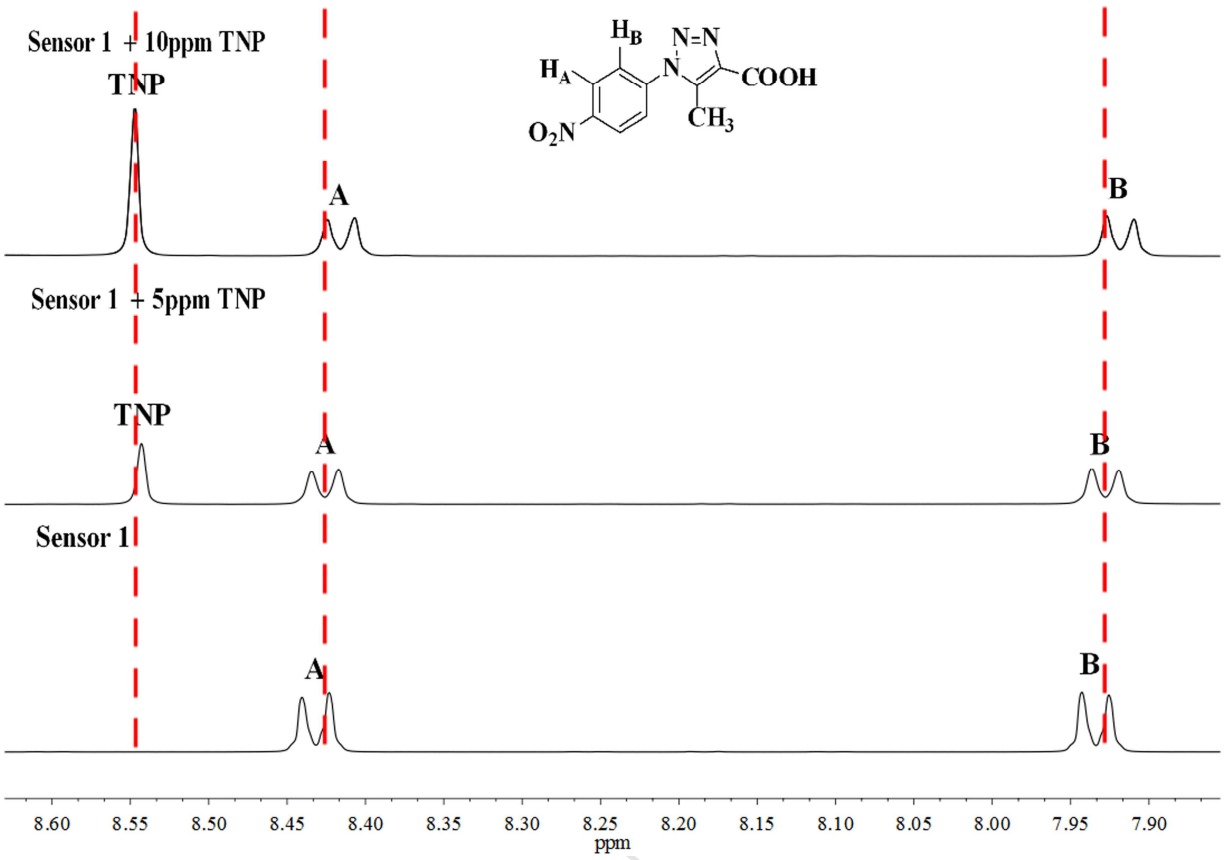

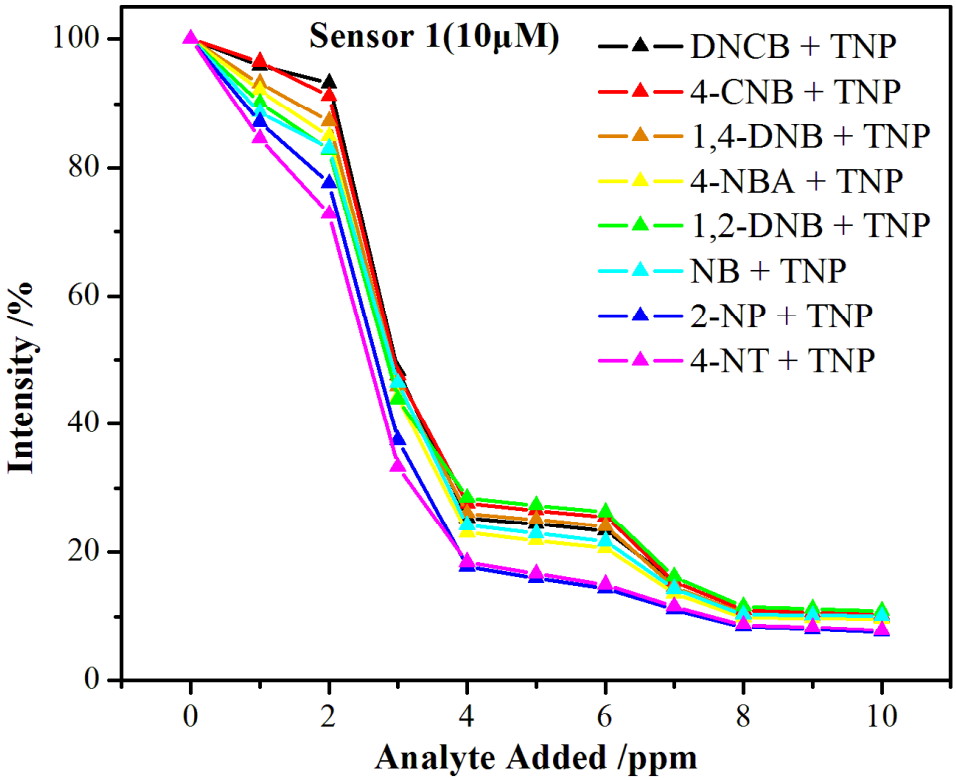

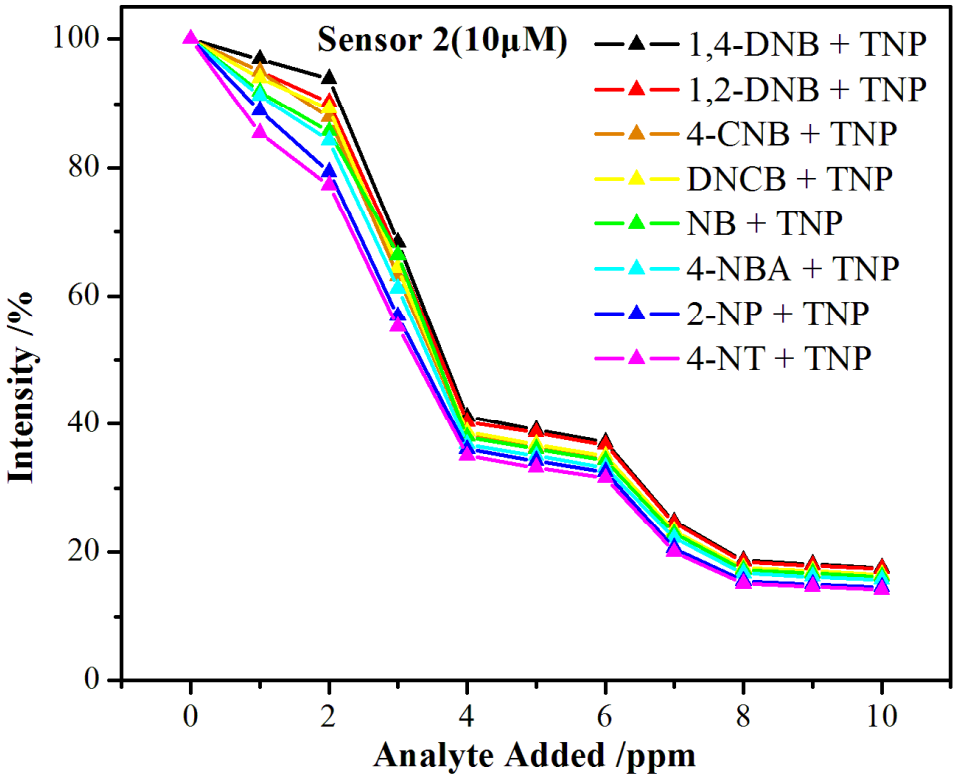

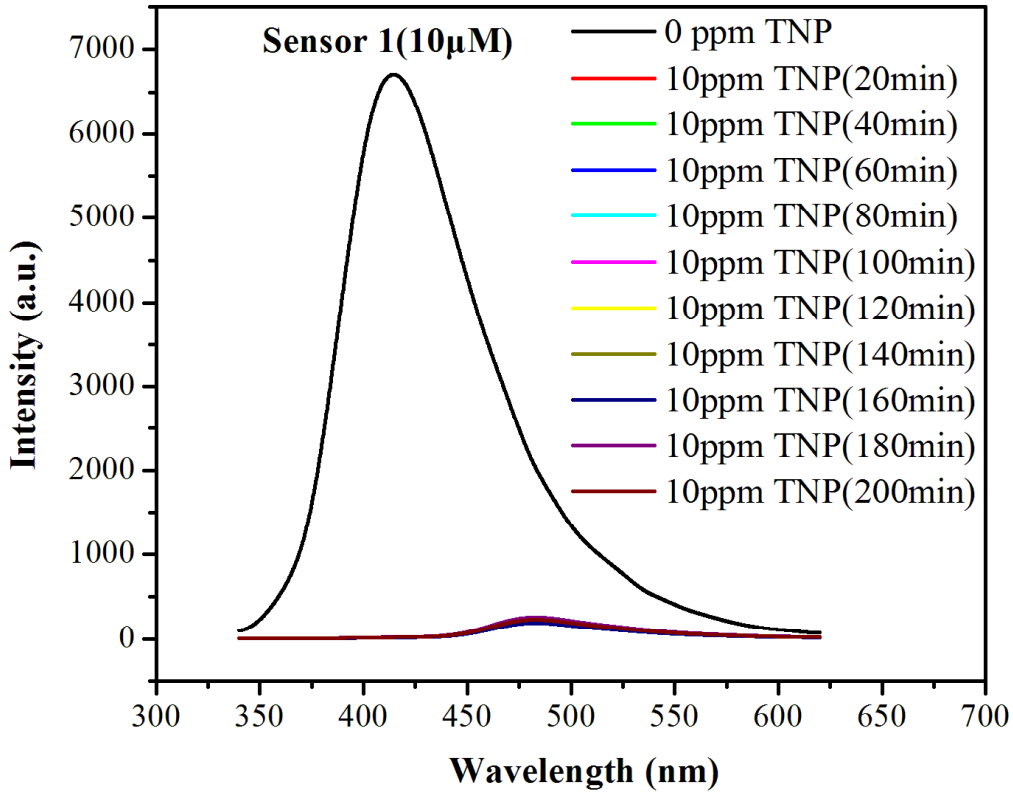

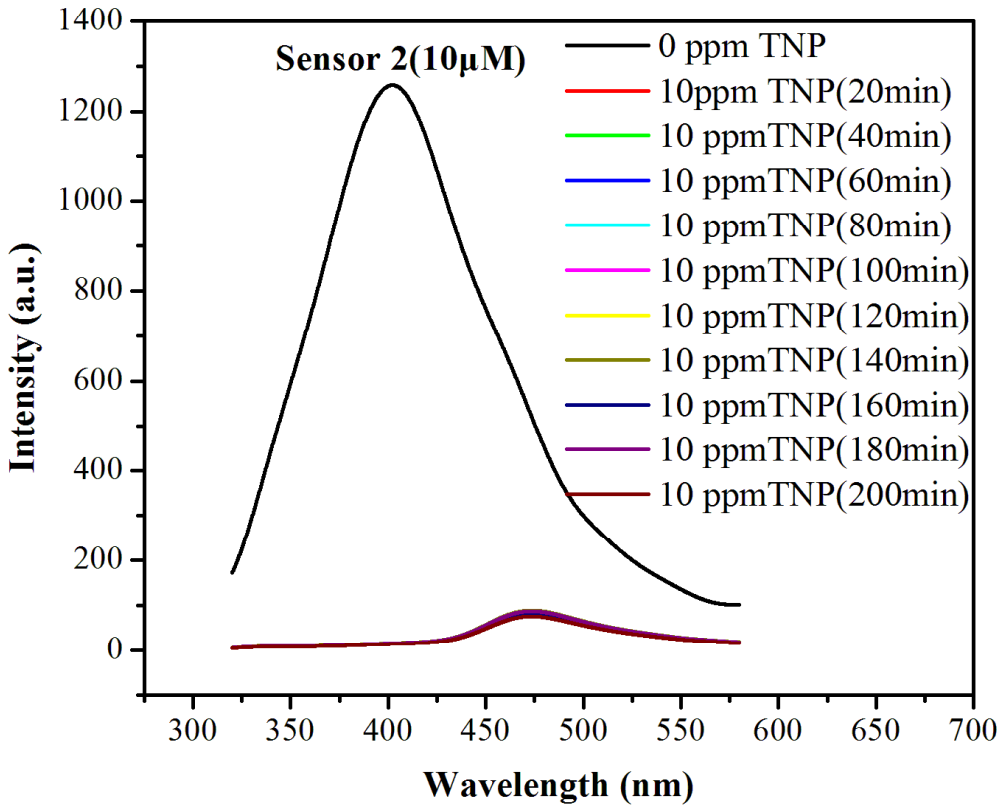

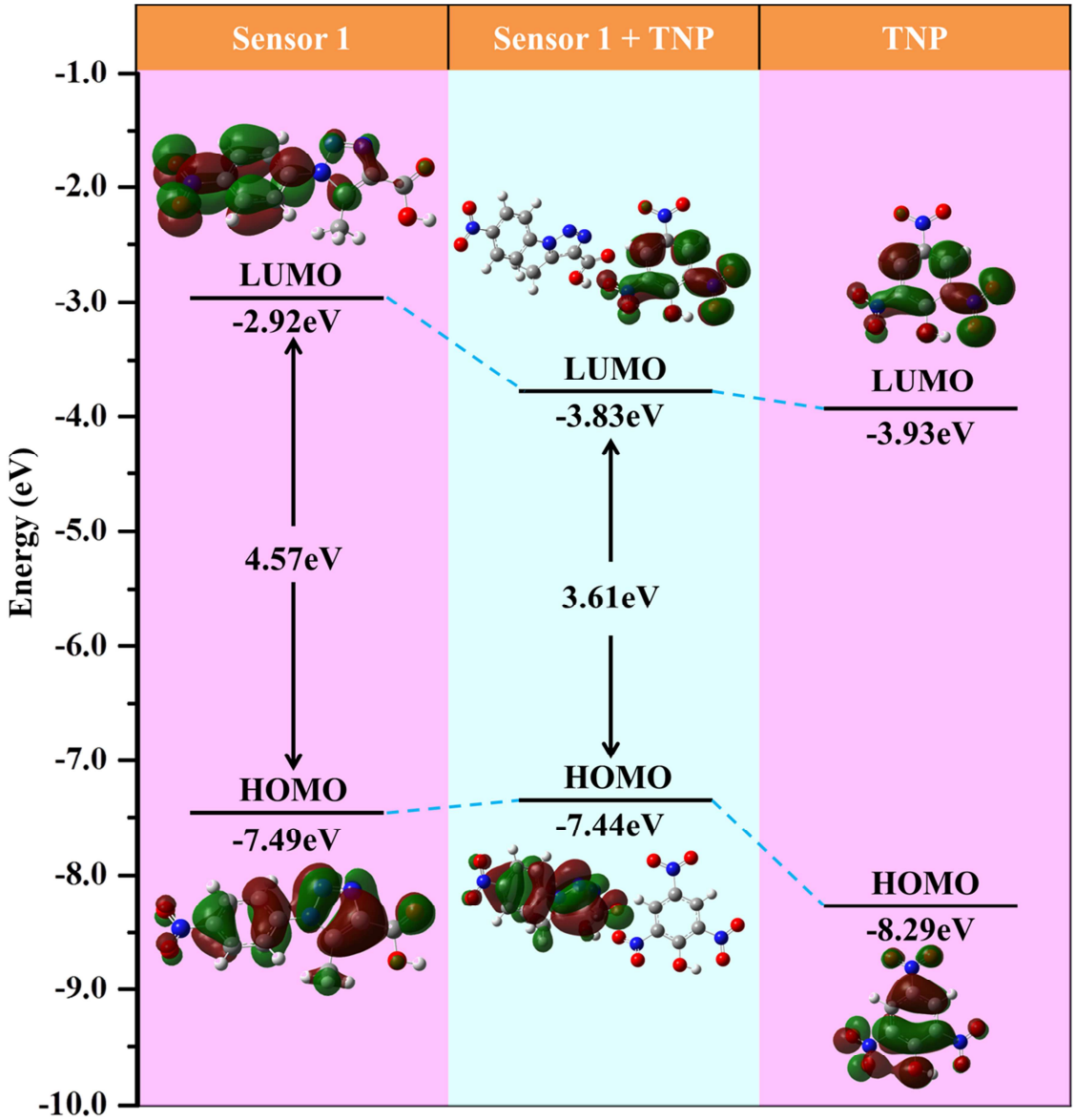
Sensor 1
Sensor 1 + TNP
TNP
Energy (eV)
-1.0
-2.0
-3.0
-4.0
-5.0
-6.0
-7.0
-8.0
-9.0
-10.0
LUMO
-2.92eV
4.57eV
HOMO
-7.49eV
LUMO
-3.83eV
3.61eV
HOMO
-7.44eV
LUMO
-3.93eV
HOMO
-8.29eV